

## Maximum Temperatures in Evolving Protoplanetary Disks and Composition of Planetary Building Blocks.

Min Li<sup>1</sup>, Shichun Huang<sup>2</sup>, Zhaohuan Zhu<sup>1</sup>, Michail I. Petaev<sup>3,4</sup>, and Jason H. Steffen<sup>1</sup>, <sup>1</sup>Department of Physics and Astronomy, University of Nevada, Las Vegas, 89154, USA, [min.li@unlv.edu](mailto:min.li@unlv.edu), [jason.steffen@unlv.edu](mailto:jason.steffen@unlv.edu) <sup>2</sup>Department of Geoscience, UNLV, 89154, USA, <sup>3</sup>Department of Earth & Planetary Sciences, Harvard University, 20 Oxford St., Cambridge 02138, USA <sup>4</sup>Harvard-Smithsonian Center for Astrophysics, 60 Garden St., Cambridge 02138, USA.

**Introduction:** In our solar system, all rocky planets [1-3] and CM, CO, and CV chondrites [4] contain near-solar proportions of refractory elements but are depleted in volatile elements [5,6].

The maximum temperature, and radial temperature profile in a protoplanetary disk is important for the condensation of different elements in the disk [7]. We simulate the evolution of a set of protoplanetary disks from the collapse of their progenitor molecular cloud cores as well as the dust decoupling within the disks as they evolve. We show how the initial properties of the cloud cores, i.e., angular velocities and temperatures, and viscosities in the disks affect the thermal history of the protoplanetary disks using a simple viscous disk model and their effects on the compositions of planetary building blocks.

**Method:** Our simulations begin with the collapse of a molecular cloud core (MCC), which self-consistently evolves into a protoplanetary disk [8]. With the distribution of initial condition of the MCC, we provide the distribution of the maximum temperatures in the disks. Then we model the condensation of elements by using chemical equilibrium calculation method.

**Disk evolution model.** We adopt the disk model used by Li & Li [8] to calculate the evolution of the disk. The evolution of surface density is

$$\frac{\partial \Sigma(R, t)}{\partial t} = \frac{3}{R} \frac{\partial}{\partial R} \left[ R^{1/2} \frac{\partial}{\partial R} (\Sigma \nu R^{1/2}) \right] + S(R, t) + S(R, t) \left\{ 2 - 3 \left[ \frac{R}{R_d(t)} \right]^{1/2} + \frac{R/R_d(t)}{1 + [R/R_d(t)]^{1/2}} \right\},$$

where  $\Sigma(R, t)$  is the surface density at radius  $R$  and time  $t$  while  $\nu$  is the kinematic viscosity,  $S(R, t)$  is the mass influx from the MCC onto the disk and protostar system [9], and  $R_d(t)$  is the centrifugal radius. In the evolving disk, we calculate the midplane temperature  $T(R, t)$  and pressure  $P(R, t)$ .

We use the  $\alpha$ -prescription [10] to calculate the viscosity, each simulation uses a constant  $\alpha$ , and the suite of simulations examines values equal to  $10^{-1}$ ,  $10^{-2}$ ,  $10^{-3}$ ,  $10^{-4}$ , and  $10^{-5}$ .

The midplane temperature in the disk is

$$\sigma T^4 = \frac{1}{2} \left[ \left( \frac{3}{8} \tau_R + \frac{1}{2\tau_p} \right) \dot{E}_v + \left( 1 + \frac{1}{2\tau_p} \right) \dot{E}_s \right] + \sigma T_{ir}^4 + \sigma T_c^4,$$

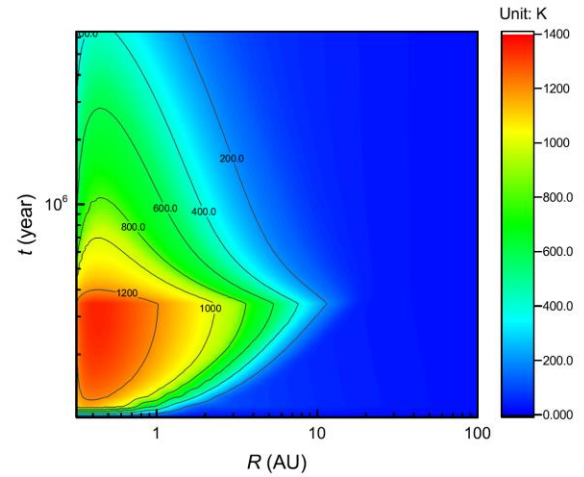
where  $\tau_R$  is the Rosseland mean optical depth and  $\kappa_R$  is the Rosseland mean opacity.

**Dust Condensation.** We use the GRAINS code [11], which assumes a full chemical equilibrium of 33 elements, to calculate the condensation of elements in the evolving disk [7]. The chemical composition of the decoupled dust was got at each radius in the disk

**Results:** The evolution of the disk was modeled with different initial conditions and viscosities.

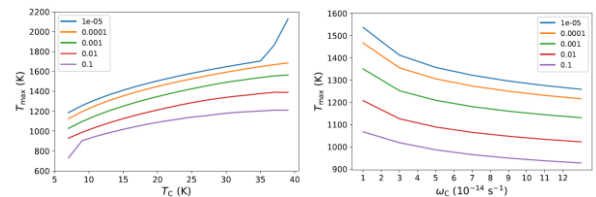
**Midplane temperatures.** We show the evolution of the midplane temperatures in the disk, the influence of initial conditions of MCC on the maximum temperatures, and the distribution of maximum temperatures from the distribution of initial conditions and viscosities.

Figure 1 shows that the midplane temperature increases first and then decreases with time within 10 AU and temperatures at larger radii peak at a later time than those at smaller radii.



**Figure 1** Contour plot of temperature as a function of radius and time. Here,  $M_c = M_{\text{Sun}}$ ,  $T_c = 15$  K,  $\omega_c = 10^{-14} \text{ s}^{-1}$ , and  $\alpha = 10^{-3}$ .

In Figure 2, we show that when the temperature of MCC increases or the angular velocity of MCC decreases, or the viscosity in the disk decreases, the maximum temperature in the disks increases.



**Figure 2** Maximum temperature as a function of  $T_c$  (left) and  $\omega_c$  (right) for different  $\alpha$ . Here  $M_c = M_{\text{Sun}}$ .

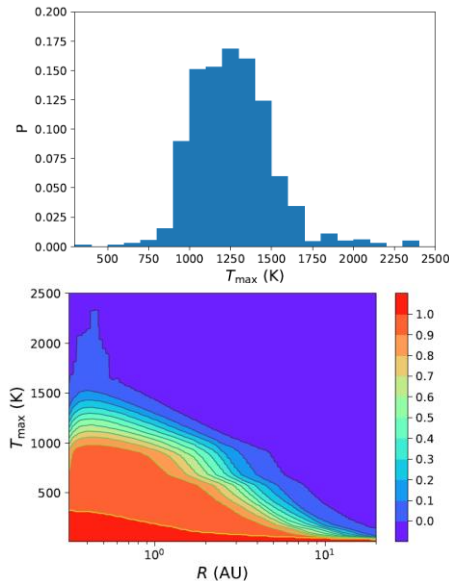


**Figure 3** Upper: Distribution of maximum temperatures achieved in our ensemble of disks. Lower: Fraction of disks that reach specific peak temperatures as a function of radius.

The distribution of maximum temperature is plot in in Figure 3. For the majority of disks in the regime of these parameters, the maximum temperature is between 1000 and 1500K, with the median value being around 1250 K. This value of the maximum midplane temperature is lower than the 50% condensation temperature of silicon at a total pressure of  $10^{-4}$  bars ( $\sim 1300$  K [7]. Generally, the maximum temperatures, and the proportions of the temperatures higher than specific values will decrease with radius.

Figure 4 shows the relative elemental abundances of decoupled elements normalized to the Solar abundance and Si as a function of 50% condensation temperature at different radii. Generally, the relative abundances of refractory elements tend to be high in disks with a high maximum temperature and their abundances decrease with time as more volatile elements condense and decouple as the temperature decreases [7]. The relative abundance of elements with 50% condensation temperatures higher than the maximum temperature at a radius are equal because they have never been vaporized.

**Conclusions:** (i) The temperature in the inner region ( $< 10$  AU) of the disk increases first and then decreases with time. It reaches its maximum value around the end of the MCC collapse (several times  $10^5$  years). (ii) The maximum temperature of the disk increases with the initial temperature of the MCC and decreases with its angular velocity. The maximum temperature in the disk also increases if the viscosity in the disk decreases since the additional material in the inner region traps more heat in the disk. (iii) 90% of the simulations that use the observed properties of MCCs predict peak temperatures between 935 and

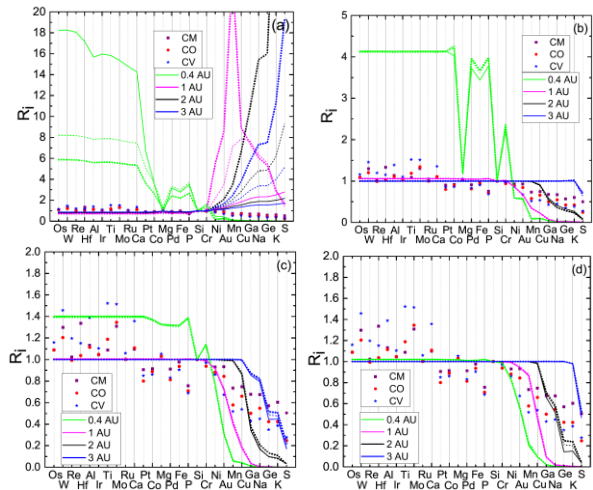


**Figure 4** Elemental abundances at different radii. (a)  $T_c=31$  K,  $\omega_c=10^{-14}$  s $^{-1}$ , and  $\alpha=10^{-5}$ . (b)  $T_c=15$  K,  $\omega_c=10^{-14}$  s $^{-1}$ , and  $\alpha=10^{-5}$ . (c)  $T_c=15$  K,  $\omega_c=10^{-14}$  s $^{-1}$ , and  $\alpha=10^{-3}$ . (d)  $T_c=15$  K,  $\omega_c=3 \times 10^{-14}$  s $^{-1}$ , and  $\alpha=10^{-3}$ .

1635 K, with a median value of 1250 K. Less than 1% of the disks from our simulations reach temperatures higher than 2000 K and are capable of vaporizing all elements. Even in these simulations, those temperatures only arise in the innermost portion of the disk. (iv) Most disks reach peak temperatures that are lower than the 50% condensation temperature of Mg. To match the depletion patterns of CM, CO, and CV chondrites and terrestrial planets, one needs either rare initial conditions of the proto-solar MCC, or other energy sources to heat the disk to very high temperatures in order to reprocess the moderately volatile to refractory elements.

**Acknowledgments:** JHS, ML, and SH are supported by the NASA grant NNX16AK08G and NSF grant AST-1910955. ZZ acknowledges support from the National Science Foundation under CAREER Grant Number AST-1753168 and Sloan Research Fellowship.

**References:** [1] Morgan J. W. and Anders E. (1980) *PNAS*, 77, 6973–6977. [2] McDonough W. F. and Sun S.-s. (1995) *Chemical Geology*, 120, 223–253. [3] Lodders K. and Fegley B. (1997) *Icarus*, 126, 373–394 [4] Wasson J. T. and Kallemeyn G. W. (1988) *Philos. Trans. R. Soc. A*, 325, 535–544 [5] Asplund M., Grevesse N., Sauval A. J., (2005), in Barnes III T. G., Bash F. N., eds, *ASPCS Vol. 336*, p. 25. [6] Asplund M., Grevesse N., Sauval A. J., Scott P. (2009) *ARA&A*, 47, 481. [7] Li M., Huang S., Petaev M. I., Zhu Z., Steffen J. H. (2020) *MNRAS*, 495, 2543 [8] Li M., Li X. (2015) *MNRAS*, 449, 2259. [9] Nakamoto T., Nakagawa Y. (1994) *ApJ*, 421, 640. [10] Shakura N. I., Sunyaev R. A. (1973) *A&A*, 500, 33. [11] Petaev M. I. (2009) *Calphad*, 33, 317–327